



Cite this: *Phys. Chem. Chem. Phys.*,  
2025, 27, 9668

## How non-aqueous media direct the reaction of $\text{Ca}(\text{OH})_2$ with $\text{CO}_2$ to different forms of $\text{CaCO}_3$ : *operando* mid-infrared and X-ray absorption spectroscopy studies†

Thokozile A. Kathyola, <sup>ab</sup> Sin-Yuen Chang, <sup>b</sup> Elizabeth A. Willneff,<sup>c</sup> Colin J. Willis,<sup>d</sup> Giannantonio Cibin,<sup>b</sup> Paul Wilson,<sup>d</sup> Anna B. Kroner, <sup>b</sup> Elizabeth J. Shotton, <sup>b</sup> Peter J. Dowding<sup>d</sup> and Sven L. M. Schroeder <sup>ab</sup>

Time-resolved structural changes taking place during the reaction of  $\text{Ca}(\text{OH})_2$  and  $\text{CO}_2$  forming different  $\text{CaCO}_3$  polymorphs, in aqueous and non-aqueous environments, were recorded *operando* using mid-infrared (mid-IR) and X-ray absorption near-edge structure (XANES) spectroscopy. Results show that  $\text{Ca}(\text{OH})_2$  directly transforms into calcite in a pure water dispersion. In methanolic media with low water content, calcium di-methylcarbonate ( $\text{Ca}(\text{OCOOCH}_3)_2$ ) is formed, which is hydrolysed to amorphous calcium carbonate (ACC) and vaterite in the presence of sufficient water. The addition of toluene shifts the equilibrium composition further from  $\text{Ca}(\text{OH})_2$  to ACC and the crystalline forms of  $\text{CaCO}_3$ , probably by affecting the activity of the methoxide intermediate. It can facilitate the formation of aragonite. No  $\text{Ca}(\text{OH})_2$  conversion was detected in pure ethanol, isopropanol and toluene dispersions, except for nanoscale  $\text{Ca}(\text{OH})_2$  in ethanolic dispersion, which formed calcium di-ethylcarbonate ( $\text{Ca}(\text{OCOOCH}_2\text{CH}_3)_2$ ). Our findings underline that vaterite formation is driven by the solution and solid state chemistry related to the reaction *via* alkoxides and carbonic acid esters of the alcohols, rather than the nucleation process in solution. The alcohol in these systems does not just act as a solvent but as a reactant.

Received 18th December 2024,  
Accepted 12th April 2025

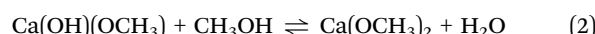
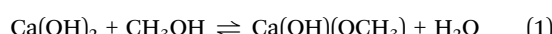
DOI: 10.1039/d4cp04774e

rsc.li/pccp

### Introduction

The molecular basis for modifying the polymorphic outcome of reactive calcium carbonate ( $\text{CaCO}_3$ ) crystallisation by choice of the solvent medium has attracted interest in various research fields, including nucleation science, biomineralisation, fuel additives, and conservation science.<sup>1–7</sup> Short-chain alcohols such as methanol, ethanol, and isopropanol are well known additives that can influence the polymorphic outcome of  $\text{CaCO}_3$  formation.<sup>8</sup> By tuning the reaction conditions in solvent systems with high alcohol content, any of the common  $\text{CaCO}_3$  forms can be obtained: amorphous  $\text{CaCO}_3$  (ACC), the metastable polymorphs vaterite and aragonite, and the thermodynamically stable polymorph calcite.<sup>5–22</sup> A mechanistic study of  $\text{CaCO}_3$  formation by reaction of  $\text{CO}_2$  with methanolic calcium

hydroxide ( $\text{Ca}(\text{OH})_2$ ) dispersions has recently provided mechanistic insight into the action of alcohols at the molecular level.<sup>23</sup> In an aqueous phase, the formation of calcite from  $\text{Ca}(\text{OH})_2$  and  $\text{CO}_2$  is the dominant reaction pathway. For high methanol contents, it is kinetically outperformed by the formation of transient methoxide and carbonate ester salts formed with methanol. The alcohol thus acts both as a reactant and a solvent/dispersant, forming the key intermediates calcium hydroxide methoxide,  $\text{Ca}(\text{OH})(\text{OCH}_3)$ , and calcium methoxide,  $\text{Ca}(\text{OCH}_3)_2$ , from  $\text{Ca}(\text{OH})_2$ .  $\text{CO}_2$  reacts with the methoxide ions to form calcium di-methylcarbonate,  $\text{Ca}(\text{OCOOCH}_3)_2$ , which transforms into an ACC sol-gel and vaterite when hydrolysed. It was confirmed that in methanolic ( $\geq 20$  mol%) systems  $\text{CaCO}_3$  forms *via* the following reaction pathways:



The formation of the  $\text{Ca}(\text{OCOOCH}_3)_2$  ester salt from methanol had occasionally been noted in the literature,<sup>24–26</sup> but its crucial mechanistic role for directing  $\text{CaCO}_3$  formation in

<sup>a</sup> School of Chemical and Process Engineering, University of Leeds, Leeds, LS2 9JT, UK. E-mail: s.l.m.schroeder@leeds.ac.uk

<sup>b</sup> Diamond Light Source, Didcot, Oxfordshire, OX11 0DE, UK

<sup>c</sup> School of Design, University of Leeds, Leeds, LS2 9JT, UK

<sup>d</sup> Infineum UK Limited, Abingdon, Oxfordshire, OX13 6BB, UK

† Electronic supplementary information (ESI) available: Figures of the experimental setup and complementary XAS, XRD and mid-IR plots. See DOI: <https://doi.org/10.1039/d4cp04774e>



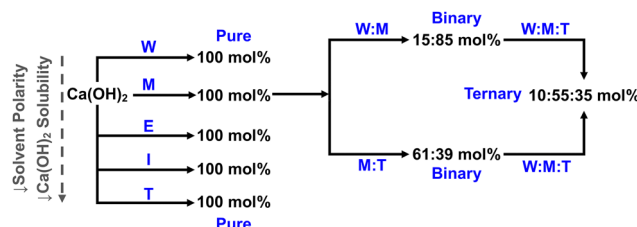


Fig. 1 Roadmap of solvent systems examined in this paper: pure, binary, and ternary water (W), methanol (M), ethanol (E), isopropanol (I), and toluene (T) systems.

methanolic phase to its metastable forms appears to have been overlooked. The hydrolysis of  $\text{Ca}(\text{OCOCH}_3)_2$  followed by diffusion-limited  $\text{ACC} \rightarrow \text{vaterite} \rightarrow \text{calcite}$  transformations was observed after stopping the addition of  $\text{CO}_2$ . Traces of aragonite were also detected. In the present paper, we will provide insight into the nature of transient species during the reactive formation of  $\text{CaCO}_3$  from  $\text{Ca}(\text{OH})_2$  and  $\text{CO}_2$  in a ternary solvent system containing methanol, water and toluene (Fig. 1).

We will also explore how higher alcohols, specifically ethanol and isopropanol, influence  $\text{CaCO}_3$  formation. Evidence for alkoxide formation in these solvents has previously been reported for nano-sized  $\text{Ca}(\text{OH})_2$  particles ('nanolimes'), which are used in art and stone conservation.<sup>5–7</sup> These studies identified the formation of calcium ethoxide and isopropoxide, but the possibility of carbonic acid ester formation was not explored. We have therefore examined the reactions in ethanol and isopropanol systems using both micro- and nano-sized  $\text{Ca}(\text{OH})_2$ .

For all system we monitored the changes in Ca speciation *in situ* and/or *operando* by a combination of mid-infrared (mid-IR) and X-ray absorption spectroscopy (XAS). XAS was, in effect, integrated into a scaled down practical reaction platform as an in-line process analytical technology (PAT) tool.<sup>27,28</sup> *In situ/operando* XAS provides deep mechanistic insight because it provides quantitative information on the nature and concentrations of transient and stable Ca species during reactions. In-line mid-IR provides complementary information on the speciation. It discriminates better than XAS between the alkoxide and ester intermediates.<sup>23</sup> As we will show, the combination of both analytical techniques leads to mechanistic scenarios explaining how alcohols determine the properties of  $\text{CaCO}_3$  products.

## Experimental

### Materials

$\text{CaCO}_3$  was synthesised using  $\text{Ca}(\text{OH})_2$  (95%; L'Hoist), ethanol, and isopropanol nanolimes (Nanorestore Plus; CSGI),  $\text{CO}_2$  (99.9%; BOC), methanol (99.9%; Fisher Scientific), and deionised water. Nitrogen (99.9%; BOC) and helium (99.9%; Air Products) were also used to control the environment during synthesis and X-ray absorption measurements respectively. Powdered samples of  $\text{Ca}(\text{OCH}_3)_2$  ( $\geq 99\%$ ; Sigma Aldrich),  $\text{Ca}(\text{OCOCH}_3)_2$ , ACC, vaterite, aragonite, and calcite ( $\geq 99\%$ ;

Sigma Aldrich) were used as references. The  $\text{Ca}(\text{OCOCH}_3)_2$ , ACC, vaterite, and aragonite were synthesised using methods previously described by Kathyola *et al.*,<sup>23</sup> Koga *et al.*,<sup>29</sup> Shikumara *et al.*,<sup>30</sup> and Kitamura *et al.*<sup>31</sup> respectively.

### Reactive crystallisation process

Dispersions were prepared by mixing micro-sized  $\text{Ca}(\text{OH})_2$  ( $\sim 30 \mu\text{m}$ ; 4.2 g) with 750 ml of solvent. Solvent ratios of the binary and ternary solvent systems (Fig. 1) were determined based on the typical synthesis methods for sulphonate-stabilised  $\text{CaCO}_3$  particles.<sup>3,32</sup> The commercial nanolimes were pre-mixed with 5 g of nano-sized  $\text{Ca}(\text{OH})_2$  ( $\sim 170 \text{ nm}$ ) dispersed in 1 L of ethanol or isopropanol. Reactions were carried out in a 1 L glass baffled reactor using a conventional lab-scale setup (Fig. S1, ESI†) under constant  $\text{N}_2$  ( $30 \text{ ml min}^{-1}$ ) flow. The temperature and stirrer speed were maintained at 28 °C and 400 rpm, respectively. Each dispersion was carbonated for a duration of 20 min using 95 wt% of the required stoichiometric amount of  $\text{CO}_2$ . The post-carbonation dispersion was stirred for a further 10 min to allow for reaction completion and growth of carbonate particles.

### Mid-IR

*Operando* mid-IR spectra were collected with a Bruker Alpha FTIR spectrometer equipped with a DPR 210 ZnSe ATR probe (Hellma Analytics) was used (Fig. S1, ESI†). Spectra were acquired from 64 scans at a resolution of  $4 \text{ cm}^{-1}$  from 4000 to  $650 \text{ cm}^{-1}$ . Measurements were controlled and data initially processed using the OPUS 7.0 software. The resulting spectra were analysed using Fityk 1.3.1 curve fitting software.<sup>33</sup>

### XAS

*Operando* fluorescence yield Ca K-edge X-ray absorption near-edge structure (XANES) spectra were collected in the photon energy range from 4000 eV to 4800 eV at beamline B18 of Diamond Light Source.<sup>34</sup> Spectra were obtained every minute before (pre-), during and after (post-) the 20 min carbonation reactions, for a total duration of 40 min. To monitor real-time chemical state changes of Ca with XAS with minimal disruption to the synthesis, a sampling loop with a bespoke multi-modal liquid jet cell was attached to the baffled reactor (Fig. S1, ESI†).<sup>27,28</sup> Aliquots of the polyphasic dispersions were continuously pumped from the reactor into the liquid jet cell and back at  $320 \text{ ml min}^{-1}$ . Data were processed and analysed using Athena in the Demeter software package.<sup>35</sup> Linear combination fitting (LCF) was performed on the *operando* spectra over a range of 4020 to 4090 eV. *Ex situ* total electron yield spectra of  $\text{Ca}(\text{OH})_2$ ,  $\text{Ca}(\text{OCH}_3)_2$ ,  $\text{Ca}(\text{OCOCH}_3)_2$ , ACC, vaterite, aragonite, and calcite reference samples were used as standards for the LCF. All measurements were acquired at room temperature under a constant He environment.

## Results and discussion

### Carbonation in pure water and in pure methanol

*Operando* mid-IR and XAS were simultaneously used to resolve the changes in Ca speciation during the 20 min carbonation of

$\text{Ca}(\text{OH})_2$  dispersed in 100 mol% water and methanol. As expected from our previous study,<sup>23</sup> the results (Fig. 2) indicated the formation of calcite and the monoester salt  $\text{Ca}(\text{OCOOCH}_3)_2$  in the water and methanol systems, respectively. In aqueous phase, calcite crystallisation was evidenced by the distinctive mid-IR absorptions associated with out-of-plane bending ( $\gamma_{\text{CO}_3}$ ) at  $871\text{ cm}^{-1}$ , asymmetric stretching ( $\nu_{\text{CO}_3}^{\text{a}}$ ) at  $1402\text{ cm}^{-1}$ , and in-plane bending ( $\delta_{\text{CO}_3}$ ) at  $710\text{ cm}^{-1}$  (Fig. 3a). These peaks are absent in the methanolic dispersion (Fig. 2b), which exhibits weak characteristic methoxycarbonyl IR absorptions arising from  $\text{C}=\text{O}$  and  $\text{C}(=\text{O})-\text{O}$  vibrational modes at  $1641\text{ (}\nu_{\text{C}=\text{O}}\text{)}, 1330\text{ (}\nu_{\text{CO}_2}^{\text{a}}\text{)}, 1095\text{ (}\nu_{\text{CO}_2}^{\text{s}}\text{)}$  and  $827\text{ (}\delta_{\text{C}=\text{O}}\text{)}\text{ cm}^{-1}$ . *Ex situ* mid-IR of the final product confirmed the formation of  $\text{Ca}(\text{OCOOCH}_3)_2$  (reactions (1)–(3)), in line with our previous findings reported for systems with high methanol content.<sup>23</sup>

Inspection of the *operando* XANES spectra (Fig. 2c and d) for both systems revealed significant changes in the features arising from  $1\text{s} \rightarrow 3\text{d}$  (at  $\sim 4040\text{ eV}$ ) and  $1\text{s} \rightarrow 4\text{p}$  (from  $4045$  to  $4060\text{ eV}$ ) electronic transitions. The expected<sup>27</sup> conversion of  $\text{Ca}(\text{OH})_2$  to calcite was detected in the aqueous dispersion (Fig. 2c). Primary indicators for this were the growth of the post-edge peak at  $4060\text{ eV}$  and a shift of about  $-2.5\text{ eV}$  in the edge position as a function of time. A similar shift was observed in the methanolic dispersion (Fig. 2d), but it was coupled with diminutions in the  $1\text{s} \rightarrow 4\text{p}$  features at about  $4045$  and  $4060\text{ eV}$ , resulting in spectra comparable to the reference  $\text{Ca}(\text{OCOOCH}_3)_2$  XANES. The post-carbonation product in methanol (at 35 min) was initially assumed to be ACC, based

on the  $1\text{s} \rightarrow 4\text{p}$  features and the relatively prominent  $1\text{s} \rightarrow 3\text{d}$  peak at  $4040\text{ eV}$ . However, this possibility was contradicted by the presence of the weak broad peak at  $4060\text{ eV}$  in the post-carbonation and  $\text{Ca}(\text{OCOOCH}_3)_2$  spectra, which is absent in the spectrum of ACC.<sup>23</sup>

The composition of the systems was further elucidated by linear combination fitting (LCF) of the XANES data. Initial fitting of the aqueous dispersion XANES (Fig. 2c) using only  $\text{Ca}(\text{OH})_2$  and calcite references resulted in what appeared to be acceptable fits, but relatively high residuals indicated that the two reference spectra were not fully accounting for the chemical speciation in the system. Inclusion of a reference spectrum of hydrated  $\text{Ca}^{2+}$  cations (obtained from a calcium chloride solution) improved the fit significantly.<sup>36</sup> It therefore appears that significant dissolution of  $\text{Ca}(\text{OH})_2$  takes place. The effect of the dissolved  $\text{Ca}^{2+}$  ions on the XANES is less apparent in the initial 5 min of the reaction due to the low solubility of  $\text{Ca}(\text{OH})_2$  in water. However,  $\text{Ca}(\text{OH})_2$  dissolution becomes more noticeable as the reaction progresses, likely due to acidification associated with the dissolution of  $\text{CO}_2$ .

LCF analysis confirmed the presence of  $\text{Ca}(\text{OCOOCH}_3)_2$  as the main product of the reaction with methanol. Attempts to include the aqueous  $\text{Ca}^{2+}$  ion spectrum in the LCF analysis of the methanolic dispersion XANES (Fig. 2d) indicated that its contribution was insignificant. Taken together, our results thus support the proposition that the post-carbonation Ca product in methanolic phase is an alkoxide and/or carbonic acid methyl ester salt.<sup>23–26</sup> Carbonate formation does not occur in the absence of water because the ester formation between  $\text{CO}_2$  and methanol is kinetically favoured over the reaction of

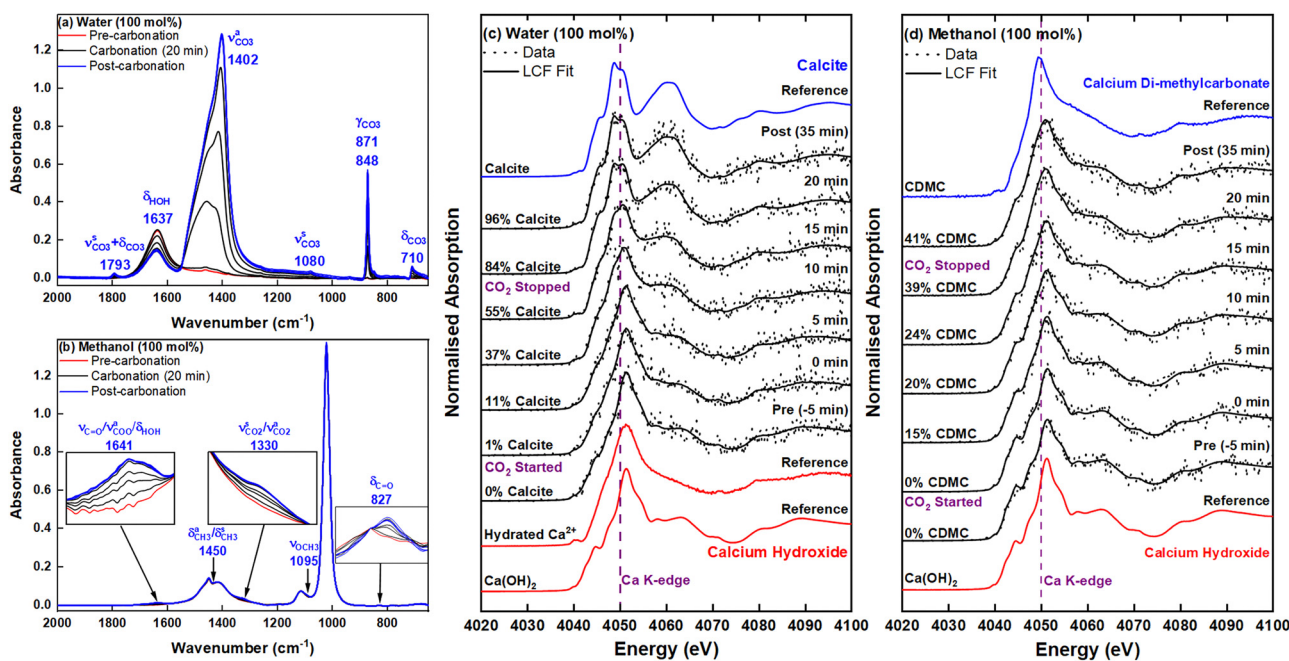
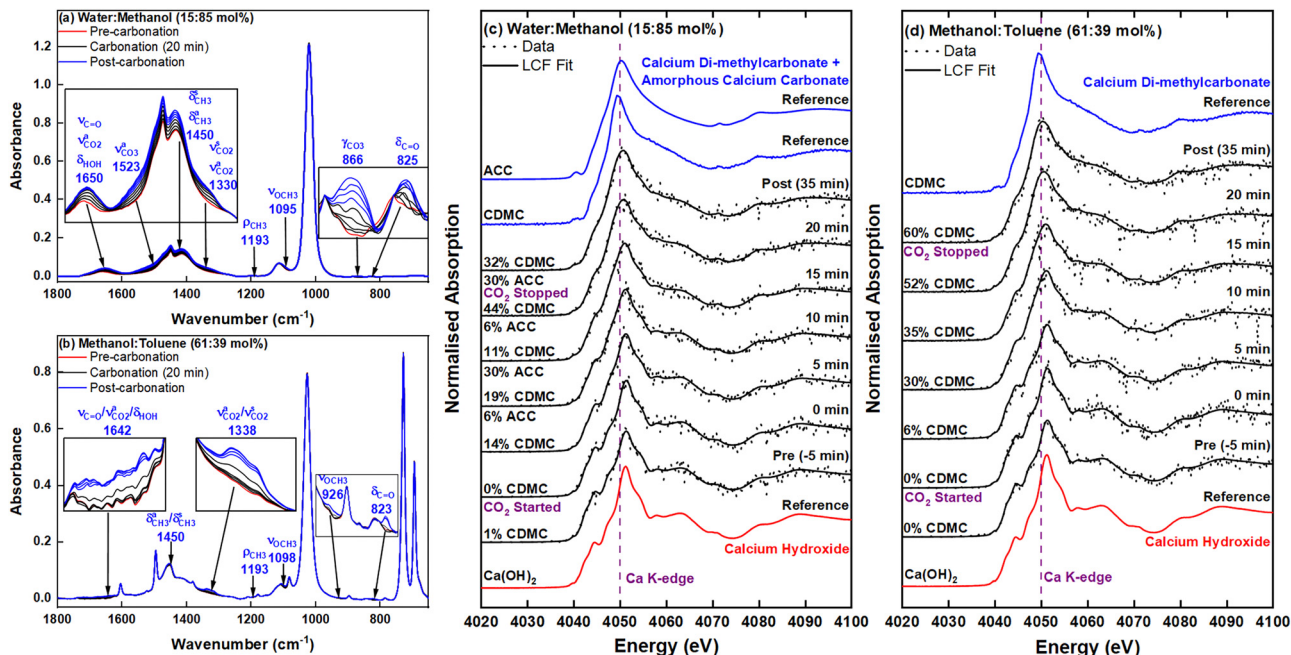


Fig. 2 *Operando* mid-IR and XANES of  $\text{Ca}(\text{OH})_2$  carbonation in pure water (a) and (c) and methanol (b) and (d) – calcite and  $\text{Ca}(\text{OCOOCH}_3)_2$  (CDMC) are formed. The full line XA spectra in (c) and (d) were obtained by LCF of the experimental spectra (dots) with the reference spectra shown at the bottom and top of the stacked plots.





**Fig. 3** Operando mid-IR and XANES of  $\text{Ca}(\text{OH})_2$  carbonation in binary solvent systems of (a) and (c) water–methanol and (b) and (d) methanol–toluene –  $\text{Ca}(\text{OCOCH}_3)_2$  (CDMC) and ACC are formed. The full line XA spectra in (c) and (d) were obtained by LCF of the experimental spectra (dots) with the reference spectra shown at the bottom and top of the stacked plots.

dissolved  $\text{CO}_2$  with the solid  $\text{Ca}(\text{OH})_2$ , which is limited by mass transport.

The accuracy of the LCF quantifications is illustrated by comparing with the expected stoichiometric amounts of calcite (Fig. 2c) and  $\text{Ca}(\text{OCOCH}_3)_2$  (Fig. 2d) with respect to the reactants. The extents of  $\text{Ca}(\text{OH})_2$  conversion were calculated based on the reported sequence of carbonation, methoxylation, and esterification (reactions (1)–(3)).<sup>23</sup> The stoichiometry of these reactions predicts that an equimolar amount of  $\text{CO}_2$  added to the two systems should result in formation of about 95% calcite and 48%  $\text{Ca}(\text{OCOCH}_3)_2$ . These values are very close to those observed through the LCF analysis of the *operando* XANES spectra, 96(4) and 41(3)%, respectively (Fig. 2). It is important to note that the absolute standard deviation values are mostly determined by the noise in the *operando* XAS data, which is caused by the mechanical instability of the liquid jet flow in the X-ray beam.<sup>27</sup>

### Binary water-methanol and methanol-toluene dispersions

As for the pure methanol system,  $\text{Ca}(\text{OCOCH}_3)_2$  was found to be the main product in the mid-IR and XANES spectra for both binary water–methanol (15:85 mol%) and methanol–toluene (61:39 mol%) systems (Fig. 3). Significant ACC was detected in the water–methanol dispersion ( $\gamma_{\text{CO}_3}$  at  $866\text{ cm}^{-1}$  in Fig. 3a) as the 15 mol% water hydrolyses  $\text{Ca}(\text{OCOCH}_3)_2$  to  $\text{CaCO}_3$  (reaction (4)).<sup>23</sup> LCF analysis of the complementary XANES (Fig. 3c) showed that the final post-carbonation product consisted of 32(7)%  $\text{Ca}(\text{OCOCH}_3)_2$  and 30(7)% ACC. Post-synthesis *ex situ* mid-IR (Fig. S2, ESI†) revealed that the mixed  $\text{Ca}(\text{OCOCH}_3)_2$ /ACC product converted into vaterite and calcite upon ageing. This is

similar to the reaction pathway previously observed in 100 and 90 mol% methanol systems, where the sequence  $\text{Ca}(\text{OCOCH}_3)_2 + \text{water} \rightarrow \text{ACC} \rightarrow \text{vaterite} \rightarrow \text{calcite}$  was found.<sup>23</sup>

In pure toluene, no significant  $\text{Ca}(\text{OH})_2$  conversion takes place at all (Fig. S3, ESI†), presumably because of the low solubilities of both  $\text{CO}_2$  and  $\text{Ca}(\text{OH})_2$  in toluene, while the solvent also acts as a barrier to mass transport of  $\text{CO}_2$  to  $\text{Ca}(\text{OH})_2$ . The LCF XANES analysis for the methanol–toluene dispersion indicated the presence of  $\text{Ca}(\text{OCOCH}_3)_2$  only, with a final composition of 60(3)% (Fig. 4d). As for pure methanol phase, no carbonate formation can take place due to the absence of water. It is sometimes assumed that no reaction at all takes place in methanol–toluene systems,<sup>37</sup> but this is clearly not supported by our data. Interestingly, both mid-IR and XANES data suggest that more  $\text{Ca}(\text{OH})_2$  is converted to  $\text{Ca}(\text{OCOCH}_3)_2$  (~60% vs. ~40% ester salt content) in the methanol–toluene system (Fig. 3b and d) compared to the pure methanol dispersion (Fig. 2b and d). It appears that the reaction equilibrium is shifted somewhat towards the ester salt in the presence of toluene, perhaps because the methoxide ion is destabilised in less polar media,<sup>38,39</sup> or because dissolution or solubilisation of the ester salt takes place in the resulting ternary system.

### Ternary water-methanol-toluene dispersion

An even higher conversion of  $\text{Ca}(\text{OH})_2$ , forming both  $\text{Ca}(\text{OCOCH}_3)_2$  and ACC, was indicated by the mid-IR for the water–methanol–toluene (10:55:35 mol%) system (Fig. 4). Analysis of the  $\gamma_{\text{CO}_3}$  deformation peak area (Fig. 4b) shows that ACC formed at a faster rate in the ternary dispersant than in the

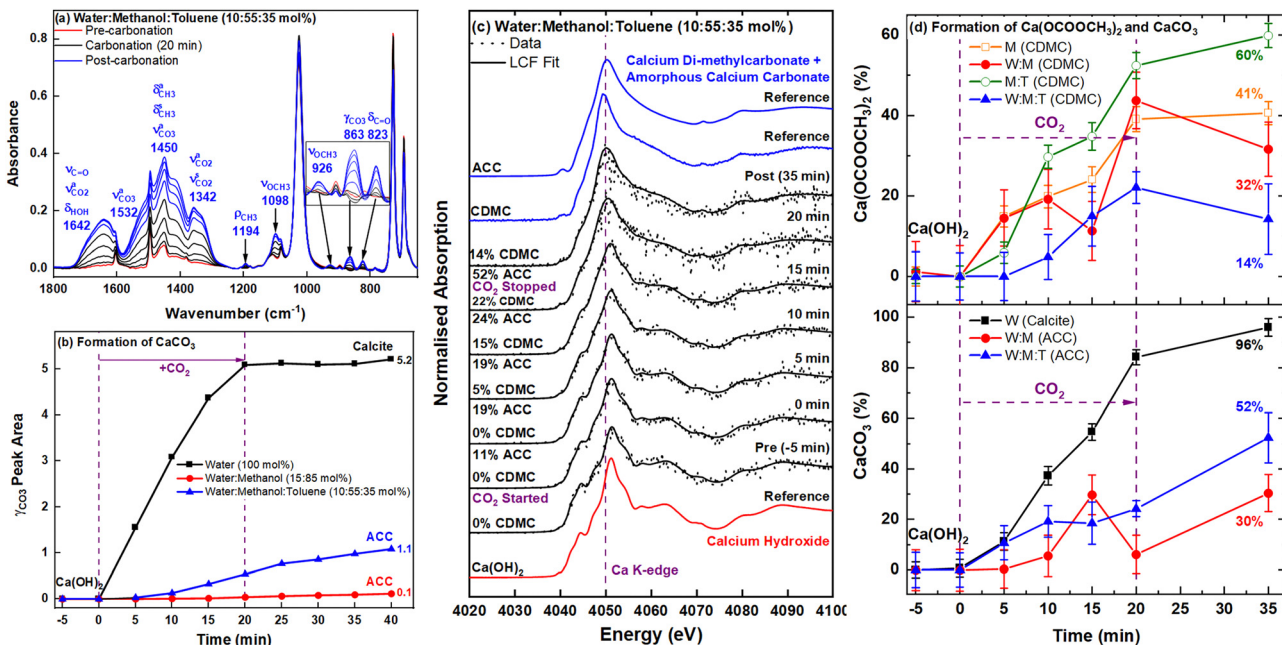


Fig. 4 Operando mid-IR and XANES of  $\text{Ca}(\text{OH})_2$  carbonation in a ternary solvent system of water–methanol–toluene (a) and (c) –  $\text{Ca}(\text{OCOOCH}_3)_2$  (CDMC) and ACC are formed; and time-resolved changes in the composition of carbonated species based on the (b) mid-IR and (d) XANES. The full line XA spectra in (c) were obtained by LCF of the experimental spectra (dots) with the reference spectra shown at the bottom and top of the stacked plots. Error bars for the XAS speciation analysis were provided from the correlation matrix of the multiparameter LCF analysis. Increased noise in the data towards the end of the XAS analysis reflect increasing jet instability due to the formation of  $\text{Ca}(\text{OCOOCH}_3)_2$  and ACC particles.

binary water–methanol system. This effect may again be related to the destabilisation of methoxide ions by the presence of the non-polar toluene molecules, which results in a higher rate of ester salt formation and subsequent hydrolysis by the water in the system (reaction (3) and (4)). The toluene also decreases the viscosity of the dispersions<sup>40</sup> and may promote diffusive mass transport of  $\text{CO}_2$  to both the methanol and  $\text{Ca}(\text{OH})_2$  components, increasing the rates further. The  $\delta_{\text{HOH}}$  peak at  $1642\text{ cm}^{-1}$  (Fig. 4a) revealed that both reactions also resulted in a significant increase in water content, above the initial 10 mol%, pushing the equilibrium further towards the hydrolysis product ACC (Fig. 3a). These conclusions are also confirmed by the LCF of the XANES (Fig. 4d) that shows about 50% less  $\text{Ca}(\text{OCOOCH}_3)_2$  in the ternary system for the majority of the reaction.

The time-dependent conversions in water, water–methanol, and water–methanol–toluene are summarised in Fig. 4b and d. All of the  $\text{Ca}(\text{OH})_2$  in the pure water system converted into  $\text{CaCO}_3$ , whereas partial conversions ( $\leq 52\%$ ) were achieved in the presence of non-aqueous solvents. According to the XANES (Fig. 4d), the final post-carbonation product from the ternary system consists of about 44% less  $\text{CaCO}_3$  than for the dispersion in pure water (Fig. 3c), reflecting the mechanistic shift to the ester hydrolysis forming ACC (reaction (4)). The  $\text{Ca}(\text{OH})_2$  conversion may also be affected by diffusion-limited precipitation due to the presence of methanol and the associated densification of the solvent media.<sup>41</sup> *Ex situ* X-ray diffraction (XRD) analysis (Fig. S4, ESI†) of the post-carbonation product from a ternary solvent dispersion with 14 times more  $\text{Ca}(\text{OH})_2$

revealed that the toluene reduced the stability of the amorphous sol–gel formed. Peaks due to calcite and vaterite were present in the initial XRD pattern of the gel (15 min post-carbonation). This is unlike the water–methanol (10 : 90 mol%) sol–gel from our previous study,<sup>23</sup> which was stable in its amorphous form up to 90 min. Interestingly, both XRD and mid-IR (Fig. S4 and S5, ESI†) for the ternary system showed that upon aging (60 hours) the  $\text{Ca}(\text{OCOOCH}_3)_2$  and ACC converted mainly into aragonite. Traces of aragonite were detected previously in the mid-IR of the aged pure methanol product, but in the presence of toluene it is the predominant polymorph. The formation of aragonite and vaterite may be attributed to kinetic stabilisation induced by solvation/adsorption of toluene. Kinetic stabilisation due to adsorption of organic compounds, such as ethanol, has been reported for these two polymorphs.<sup>6,8,42</sup> Additionally, toluene has been shown to affect the surface structure of  $\text{Ca}(\text{OH})_2$ .<sup>43</sup> Toluene may perhaps be behaving like  $\text{Mg}^{2+}$  ions in restricting crystal growth and preventing the formation of calcite whilst promoting that of aragonite.<sup>42,44</sup>

#### Pure ethanol and isopropanol dispersions

Carbonation in the presence of ethanol and isopropanol was associated with no significant changes in the mid-IR (Fig. S6, ESI†) and XANES (Fig. 5) when standard coarse grained ( $\sim 30\text{ }\mu\text{m}$  particle size)  $\text{Ca}(\text{OH})_2$  was carbonated in the presence of pure ethanol and isopropanol. Compared to methanol,  $\text{Ca}(\text{OH})_2$  has lower solubility in the ethyl and isopropyl alcohols, reducing the rate of carbonation reaction.<sup>45,46</sup>



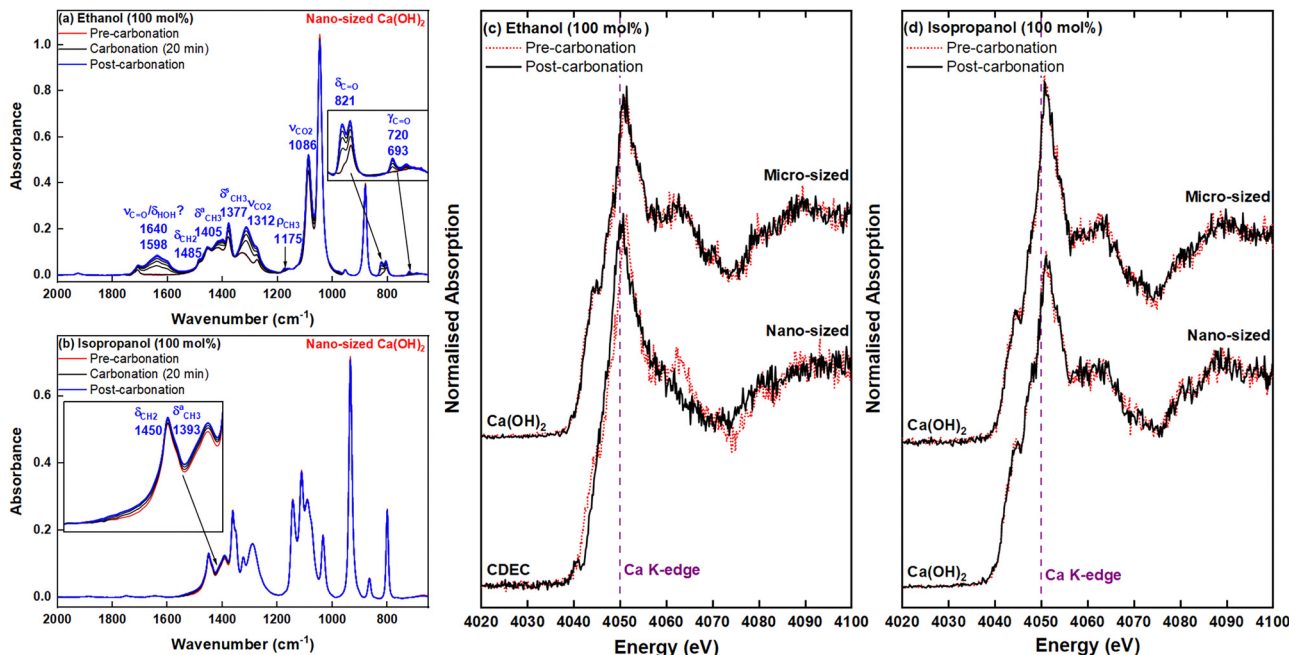


**Fig. 5** Operando mid-IR and XANES of the carbonation of micro- and nano-sized  $\text{Ca}(\text{OH})_2$  in pure ethanol (a) and (c) and isopropanol (b) and (d) –  $\text{Ca}(\text{OCOOCH}_2\text{CH}_3)_2$  (CDEC) and traces of  $\text{Ca}(\text{OCOOCH}_2\text{CH}_2\text{CH}_3)_2$  (in mid-IR only) are formed.

Nonetheless, the formation of calcium ethoxide and isopropoxide has been reported in alcoholic dispersions of nano-sized ( $\sim 170$  nm)  $\text{Ca}(\text{OH})_2$ .<sup>5–7</sup> In analogy to the methanolic systems discussed above, these alkoxide salts were identified as precursors for ACC and vaterite. Analysis of the mid-IR (Fig. 5a) for ethanol solutions of nanolimes shows evidence for the conversion of the nano-sized  $\text{Ca}(\text{OH})_2$  to calcium di-ethylcarbonate,  $\text{Ca}(\text{OCOOCH}_2\text{CH}_3)_2$ . This was determined from the peak assignments for the previously discussed  $\text{Ca}(\text{OCOOCH}_3)_2$  ester and literature data on the ethoxycarbonyl ( $-\text{COOCH}_2\text{CH}_3$ ) group.<sup>23,47</sup> Some minor changes were observed in the isopropanol mid-IR (Fig. 5b), which could be due to the formation of calcium di-isopropylcarbonate,  $\text{Ca}(\text{OCOOCH}_2\text{CH}_2\text{CH}_3)_2$ .

LCF analysis of the XANES (Fig. 5c and d) for the ethanol and isopropanol systems was not possible due to the lack of reference spectra for the respective ester intermediates. However, a qualitative comparison of the pre- and post-carbonation spectra clearly shows that conversion from  $\text{Ca}(\text{OH})_2$  only occurred in the ethanol nanolimes system. Ultimately, these results show that increasing the alkyl chain length decreases the reactivity of the alcohol and that  $\text{Ca}(\text{OH})_2$  particle size has a significant influence on the reaction rate. Formation of carbonated Ca species in the ethanol system is comparable to methanol only when the  $\text{Ca}(\text{OH})_2$  particle size is sufficiently reduced to overcome the mass transport limitations associated with the lower ester concentration in the mixtures.

## Conclusions

Combined *operando* mid-IR and XAS studies of multiphase multicomponent  $\text{CaCO}_3$  crystallisation from  $\text{Ca}(\text{OH})_2$  and  $\text{CO}_2$

were carried out. The rates of  $\text{Ca}(\text{OH})_2$  conversion to different  $\text{CaCO}_3$  forms were monitored in real-time in various solvent systems, including pure and mixed systems of water, methanol, ethanol, isopropanol, and toluene. Calcite was confirmed to be the final product in pure water (100 mol% water). In methanolic systems with low water content the formation of the carbonate ester salt  $\text{Ca}(\text{OCOOCH}_3)_2$  dominates. It hydrolyses to ACC and vaterite in the presence of water. The addition of toluene to methanol/water systems increased reaction rates of ester formation, indicating destabilisation of the methoxide intermediate by the non-polar solvent, and facilitated the crystallisation of aragonite. No conversion of crystalline  $\text{Ca}(\text{OH})_2$  to carbonic acid alkyl ester salts was observed in pure ethanol and isopropanol dispersions, except when highly dispersed ('nanolime')  $\text{Ca}(\text{OH})_2$  was contacted with the alcohol. For this case, the formation of  $\text{Ca}(\text{OCOOCH}_2\text{CH}_3)_2$  and traces of  $\text{Ca}(\text{OCOOCH}_2\text{CH}_2\text{CH}_3)_2$  were detected. Overall, the results show that depending on solvent composition the carbonated ester intermediate can transform into various forms of  $\text{CaCO}_3$ . The most prevalent polymorphs are ACC, vaterite and calcite, but aragonite can be accessed by the addition of toluene. The examination of the nanolimes indicated that ethanol is probably a viable replacement for methanol only when the  $\text{Ca}(\text{OH})_2$  particle size is reduced to the nano-scale.

## Author contributions

All authors contributed to the work presented in this paper. T. A. K., S.-Y. C., E. A. W., C. W., G. C., A. B. K., P. J. D. and S. L. M. S. contributed to the conception and design of the experiments. C. W., G. C., P. W. and A. B. K. provided technical



support. T. A. K., S.-Y. C., E. A. W., C. W., P. W., E. J. S., P. J. D. and S. L. M. S. performed the experiments. T. A. K. analysed the data and wrote the manuscript, which was edited by E. A. W. and S. L. M. S.

## Data availability

All data supporting this study are provided either in the Results section of this paper or in the ESI,† accompanying it.

## Conflicts of interest

There are no conflicts to declare.

## Acknowledgements

This research was supported by Infineum UK Ltd., the Royal Academy of Engineering, Diamond Light Source (DLS; Beamtime Awards – SP14673 and SP21040), the EPSRC Centre for Doctoral Training in Complex Particulate Products and Processes, cP<sup>3</sup> (Grant Number – EP/L015285/1) and EPSRC Future Continuous Manufacturing and Advanced Crystallisation (CMAC) Research Hub (Grant Number – EP/P006965/1). T. A. K. gratefully acknowledges financial support from cP<sup>3</sup>, University of Leeds (UoL), Infineum UK Ltd., and the CMAC Research Hub. S. L. M. S. acknowledges the support of the Bragg Centenary Chair by the Royal Academy of Engineering, Infineum UK Ltd., and DLS. Thanks to Matthew Guindy (UoL), Arturs Pugejs (UoL), Robert W. M. Hooley (UoL) and Samuel G. Booth for their aid with some of the data collection; and Muling Zeng (UoL) for the ACC sample.

## References

- 1 F. C. Meldrum and H. Colfen, *Chem. Rev.*, 2008, **108**, 4332–4432.
- 2 J. F. Marsh, *Chem. Ind.*, 1987, **14**, 470–473.
- 3 J. P. Roman, P. Hoornaert, D. Faure, C. Biver, F. Jacquet and J. M. Martin, *J. Colloid Interface Sci.*, 1991, **144**, 324–339.
- 4 C. Belle, R. Gallo, F. Jacquet, P. Hoornaert and J. P. Roman, *Lubr. Sci.*, 1992, **5**, 11–31.
- 5 C. Rodriguez-Navarro, A. Suzuki and E. Ruiz-Agudo, *Langmuir*, 2013, **29**, 11457–11470.
- 6 C. Rodriguez-Navarro, K. Elert and R. Sevcik, *CrystEngComm*, 2016, **18**, 6594–6607.
- 7 C. Rodriguez-Navarro, I. Vettori and E. Ruiz-Agudo, *Langmuir*, 2016, **32**, 5183–5194.
- 8 K. K. Sand, J. D. Rodriguez-Blanco, E. Makovicky, L. G. Benning and S. L. S. Stipp, *Cryst. Growth Des.*, 2012, **12**, 842–853.
- 9 T. Yasue, A. Mamiya, Y. Takahashi, R. Tsukisaka and Y. Arai, *Nippon Kagaku Kaishi*, 1984, **1984**, 1107–1113.
- 10 T. Yasue, A. Mamiya, T. Fukushima and Y. Arai, *Gypsum Lime*, 1985, **1985**, 245–252.
- 11 Y. Ueda, K. Komatu, S. Shimizu, H. Nishioka, M. Hanazaki and S. Minayoshi, *Gypsum Lime*, 1994, **1994**, 105–114.
- 12 F. Manoli and E. Dalas, *J. Cryst. Grow.*, 2000, **218**, 359–364.
- 13 S. R. Dickinson and K. M. McGrath, *J. Mater. Chem.*, 2003, **13**, 928–933.
- 14 J.-K. Park, J.-W. Ahn, Y.-S. Park and C. Han, *Geosyst. Eng.*, 2004, **7**, 89–94.
- 15 K. S. Seo, C. Han, J. H. Wee, J. K. Park and J. W. Ahn, *J. Cryst. Grow.*, 2005, **276**, 680–687.
- 16 H. S. Lee, T. H. Ha and K. Kim, *Mater. Chem. Phys.*, 2005, **93**, 376–382.
- 17 S. F. Chen, S. H. Yu, J. Jiang, F. Q. Li and Y. K. Liu, *Chem. Mater.*, 2006, **18**, 115–122.
- 18 S. F. Chen, H. Colfen, M. Antonietti and S. H. Yu, *Chem. Commun.*, 2013, **49**, 9564–9566.
- 19 Y. D. Hu, Y. H. Zhou, X. R. Xu and R. K. Tang, *Cryst. Res. Technol.*, 2015, **50**, 312–318.
- 20 G. Magnabosco, I. Polishchuk, B. Pokroy, R. Rosenberg, H. Colfen and G. Falini, *Chem. Commun.*, 2017, **53**, 4811–4814.
- 21 M. Farhadi-Khouzani, D. M. Chevrier, P. Zhang, N. Hedin and D. Gebauer, *Angew. Chem., Int. Ed.*, 2016, **55**, 8117–8120.
- 22 Y. Nakashima, C. Takai, H. Razavi-Khosroshahi, W. Suthabanditpong and M. Fuji, *Adv. Powder Technol.*, 2018, **29**, 904–908.
- 23 T. A. Kathyola, E. A. Willneff, C. J. Willis, P. J. Dowding and S. L. M. Schroeder, *ACS Phys. Chem. Au*, 2024, **4**, 555–567.
- 24 A. Buzágh, *Kolloidn. Z.*, 1926, **38**, 222–226.
- 25 J. Plank, H. Hoffmann, J. Schölkopf, W. Seidl, I. Zeitler and Z. Zhang, *Res. Lett. Mater. Sci.*, 2009, **2009**, 1–3.
- 26 G. J. Witkamp, S. A. P. Escobar and R. S. Gaertner, *US Pat.*, 20150344319A1, 2015.
- 27 S. Y. Chang, T. A. Kathyola, E. A. Willneff, C. J. Willis, P. Wilson, P. J. Dowding, G. Cibin, A. B. Kroner, E. J. Shotton and S. L. M. Schroeder, *React. Chem. Eng.*, 2019, **4**, 679–687.
- 28 T. A. Kathyola, S.-Y. Chang, E. A. Willneff, C. J. Willis, G. Cibin, P. Wilson, A. B. Kroner, E. J. Shotton, P. J. Dowding and S. L. M. Schroeder, *Ind. Eng. Chem. Res.*, 2023, **62**, 16198–16206.
- 29 N. Koga, Y. Z. Nakagoe and H. Tanaka, *Thermochim. Acta*, 1998, **318**, 239–244.
- 30 C. Shrivikrama, P. Singh, A. Gupta and M. S. Hegde, *Mater. Res. Bull.*, 2006, **41**, 1455–1460.
- 31 M. Kitamura, H. Konno, A. Yasui and H. Masuoka, *J. Cryst. Grow.*, 2002, **236**, 323–332.
- 32 I. Markovic, R. H. Ottewill, D. J. Cebula, I. Field and J. F. Marsh, *Colloid Polym. Sci.*, 1984, **262**, 648–656.
- 33 M. Wojdyr, *J. Appl. Crystallogr.*, 2010, **43**, 1126–1128.
- 34 A. J. Dent, G. Cibin, S. Ramos, A. D. Smith, S. M. Scott, L. Varandas, M. R. Pearson, N. A. Krumpa, C. P. Jones and P. E. Robbins, *J. Phys. Conf. Ser.*, 2009, **190**, 012039.
- 35 B. Ravel and M. Newville, *J. Synchrotron Radiat.*, 2005, **12**, 537–541.
- 36 J. L. Fulton, S. M. Heald, Y. S. Badyal and J. M. Simonson, *J. Phys. Chem. A*, 2003, **107**, 4688–4696.
- 37 M. L. Robbins, F. Leder, E. Chludzinski and G. R. Chludzinski, *US Pat.*, 3429811A, 1969.



38 J. I. Brauman and L. K. Blair, *J. Am. Chem. Soc.*, 1968, **90**, 6561–6562.

39 J. I. Brauman and L. K. Blair, *J. Am. Chem. Soc.*, 1970, **92**, 5986–5992.

40 U. B. Bray, C. R. Dickey and V. Voorhees, *Ind. Eng. Chem. Prod. Res. Dev.*, 1975, **14**, 295–298.

41 Y. Oaki and H. Imai, *Cryst. Growth Des.*, 2003, **3**, 711–716.

42 F. C. Meldrum, *Int. Mater. Rev.*, 2003, **48**, 187–224.

43 I. Pashalidis and C. R. Theocaris, *J. Chem. Technol. Biotechnol.*, 1998, **71**, 223–226.

44 Y. Kitano, D. W. Hood and K. Park, *J. Geophys. Res.*, 1962, **67**, 4873.

45 A. Seidell, *Solubilities of Inorganic and Organic Compounds: A Compilation of Solubility Data from the Periodical Literature*, D. Van Nostrand Company, New York, 1919.

46 G. Just, *Z. Phys. Chem.*, 1901, **37**, 342–367.

47 N. P. G. Roeges, in *Guide to the complete interpretation of infrared spectra of organic structures*, ed. A. N. Lobachev, John Wiley & Sons Ltd., Chichester, England, 1994, pp. 263–269.